PHOTONICS Research

Phonon lasing in a hetero optomechanical crystal cavity

Kaiyu Cui,[1,2,*,†] Zhilei Huang,[1,†] Ning Wu,[1,2] Qiancheng Xu,[1,2] Fei Pan,[1,2] Jian Xiong,[1,2] Xue Feng,[1,2] Fang Liu,[1,2] Wei Zhang,[1,2,3] and Yidong Huang[1,2,3]

[1]Department of Electronic Engineering, Tsinghua University, Beijing 100084, China
[2]Beijing National Research Center for Information Science and Technology (BNRist), Tsinghua University, Beijing 100084, China
[3]Beijing Academy of Quantum Information Science, Beijing, China
*Corresponding author: kaiyucui@tsinghua.edu.cn

Micro- and nanomechanical resonators have emerged as promising platforms for sensing a broad range of physical properties, such as mass, force, torque, magnetic field, and acceleration. The sensing performance relies critically on the motional mass, mechanical frequency, and linewidth of the mechanical resonator. Herein, we demonstrate a hetero optomechanical crystal (OMC) cavity based on a silicon nanobeam structure. The cavity supports phonon lasing in a fundamental mechanical mode with a frequency of 5.91 GHz, an effective mass of 116 fg, and a mechanical linewidth narrowing in the range from 3.3 MHz to 5.2 kHz, while the optomechanical coupling rate is as high as 1.9 MHz. With this phonon laser, on-chip sensing can be predicted with a resolution of $\delta\lambda/\lambda = 1.0 \times 10^{-8}$. The use of a silicon-based hetero OMC cavity that harnesses phonon lasing could pave the way toward high-precision sensors that allow silicon monolithic integration and offer unprecedented sensitivity for a broad range of physical sensing applications. © 2021 Chinese Laser Press

1. INTRODUCTION

Micro- and nanomechanical resonators, allowing the detection of mass [1–4], force [5–7], torque [8], magnetic field [9,10], and acceleration [11] with ultrahigh sensitivity and over a large dynamic range, can be extensively used for spectrometry, chemical analyses, biomedical diagnoses, and in consumer electronics. In particular, it is possible to drive and quantify mechanical motion via optical-only operations in optomechanical systems, thus creating possibilities for monolithic integration. Among a variety of optomechanical candidates that include whispering gallery mode cavities [12–14] and membrane resonators [15], optomechanical crystal (OMC) cavities [16] are excellent candidates for use in sensing. This is because OMC cavities enable strong optomechanical interaction (~100 kHz) with high mechanical frequency (~GHz) and low-motional mass (~100 fg) [17,18]. A low-motional mass benefits the detection of minute masses [19–21], while an increased mechanical frequency results in increased resistance to environmental disturbances [17,20,21] and to a larger sensing bandwidth [11]. For increased sensitivity in sensing, it is capable of detecting mechanical motion with an imprecision at (or below) the standard quantum limit [5,7,22]. Unfortunately, this generally tends to be unattainable in the ambient environment of a practical setting with significantly increased mechanical dissipation [6,23–25]. This is because the sensing

mechanisms that rely on the detection of the mechanical resonance shift depend critically on the mechanical linewidth or the mechanical Q-factor [19]. Efforts have been expended to effectively reduce the damping loss from mechanical vibrations and thus increase the mechanical Q-factor to values of the order of 10^6 through the use of vacuum [11] or cryogenic measurements [18]. However, vacuum or cryogenic conditions pose substantial technical challenges and limit usefulness for practical applications [26].

In an optomechanical cavity, light can interact with the mechanical motion and affect the effective mechanical damping rate [17]. When the pump light is blue-detuned and its power increases, the effective mechanical damping can be reduced to values below zero, and even coherent self-sustained oscillation, that is, phonon lasing, can occur [27]. Thus, by applying dissipative feedback [5,6] based on the radiation pressure of the blue-detuned pump light, the constraint of mechanical damping on the mechanical linewidth in the ambient environment can be partially relaxed [28] for ultraprecise sensing applications. Upon further increases of the power of the pump light, highly coherent optomechanical oscillation with a narrow mechanical linewidth can be achieved if the mechanical motion is excited coherently. Recently, this type of oscillation has been induced in a silica microsphere for optomechanical spring sensing of a single molecule [3]. Despite these advances, the

harnessing of pronounced phonon laser for sensing applications has remained elusive thus far. Integrating this optomechanical sensing capability into silicon would enable high-precision sensing in a system that can be integrated with other multifunctional on-chip devices.

In this study, we demonstrate a phonon laser with a hetero OMC cavity in silicon. The heterostructure consists of two periodic substructures that separately confine the optical and mechanical defect modes in a nanobeam cavity. Based on our heterostructure approach, we obtained a mechanical frequency of 5.91 GHz and a motional mass of 116 fg when the optical mode was maintained at 1573.5 nm. Using this device, the optomechanical coupling rate of the cavity was measured to be 1.9 MHz, and phonon lasing was achieved with a coupled optical input power of 31 μW. The mechanical damping loss was dramatically reduced as the linewidth narrowing changed from 3.3 MHz to 5.2 kHz after phonon lasing, corresponding to an effective mechanical Q-factor boosting from 1.8×10^3 to 1.1×10^6. Accordingly, ultra-precise sensing using the phonon laser is predicted with a resolution as high as $\delta\lambda/\lambda = 1.0 \times 10^{-8}$.

2. RESULTS

A. Hetero OMC Cavity

The hetero OMC [29], which consists of two periodic structures (P-I and P-II), was designed to overcome the design constraints of the optical and mechanical properties in an identical periodic structure of conventional OMC. By concatenating P-I and P-II with a defect region in a 1D silicon nanobeam, a hetero OMC cavity was formed [Fig. 1(a)]. The oblique view

of a unit cell of the periodic silicon block structure with a circular air hole is shown in the inset of Fig. 1(a). The unit cell can be determined by four geometric parameters, including height (h), width (w), radius of air hole (r), and length (d), which correspond to the pitch of the periodic structure. P-I and P-II both consisted of five unit cells and possessed an h value of 220 nm and a w value of 460 nm, r was 136 nm for P-I and 88 nm for P-II, while d was 493 nm for P-I and 400 nm for P-II. Owing to the difference in geometry, the P-I and P-II structures formed the hetero OMC.

In the defect region, the radius of air holes and the spacing between the holes decreased linearly in steps of 10 and 40 nm, respectively, from the side to the center. Profiles of the optical and mechanical modes of the cavity are shown in Figs. 1(b) and 1(c), respectively. The mechanical frequency of the cavity reached 5.91 GHz but maintained the optical mode at 1573.5 nm, which corresponded to a frequency of 190.5 THz. Based on the mechanical mode profile, the motional mass [17] for the confined mechanical mode was calculated to be 116 fg.

The confinement mechanism for the optical and mechanical modes in the hetero structure can be analyzed using the photonic and phononic bands formed by the two periodic structures. The photonic band structures in this study were calculated using the plane wave expansion method. Other simulations, including those of the phononic bands and the optical and mechanical modes, were performed using the finite element method. Figures 1(d) and 1(e) show the TE photonic and y-, z-symmetric phononic band diagrams of these two periodic structures. Owing to the differences in geometry, the P-I and P-II structures possess different photonic and phononic
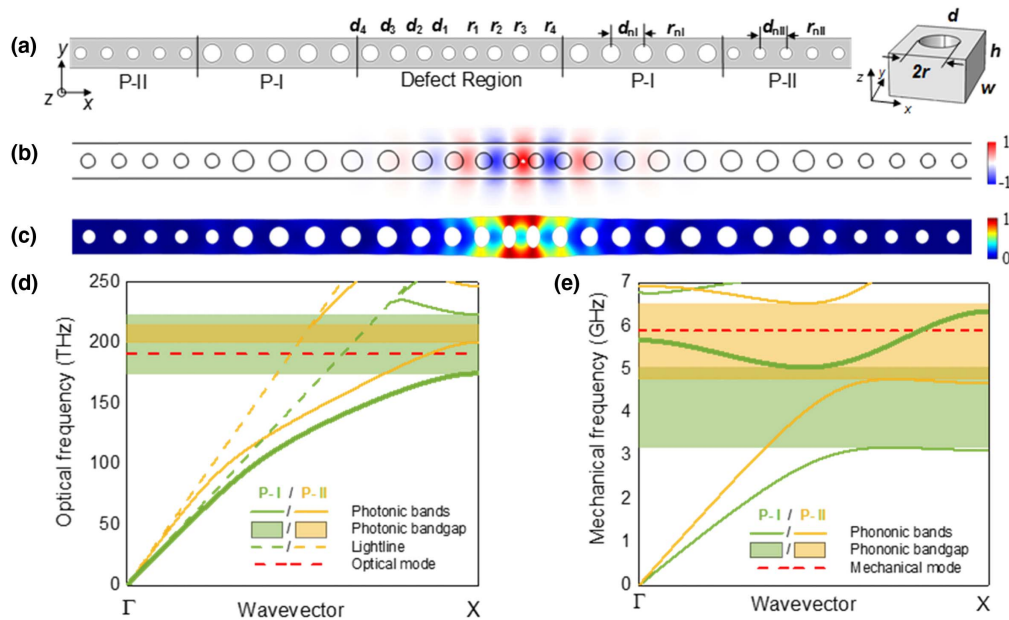

Fig. 1. (a) Top-view schematic of the hetero optomechanical crystal (OMC) cavity. Inset shows an oblique view of the unit cell that forms the periodic structure. The unit cell can be determined by four geometric parameters, namely, the height (h), width (w), radius of the air hole (r), and length (d), which correspond to the pitch of the periodic structure. (b) Mode profile of the electric y-component of the optical mode and (c) that of the displacement of the mechanical mode. (d), (e) TE optical bands and y- and z-symmetric mechanical bands of the P-I (green) and P-II (yellow) structures, respectively. The red dashed lines in (d) and (e) represent the frequency of the optical and mechanical modes, respectively. Owing to the unequal period of the P-I and P-II structures, the X points correspond to different wavevectors, and the light lines of the P-I (yellow dashed line) and P-II (green dashed line) structures do not overlap in the photonic band diagram.

bands. The green color represents the P-I structure, and the yellow color represents the P-II structure. Given that the period and hole radius of P-II are smaller than those of P-I, the central frequency of the photonic bandgap of P-II is higher, while the range is smaller, as shown in Fig. 1(d). The smaller period and hole radius of the P-II structure also contributed to a higher frequency for the mechanical bandgap, as shown in Fig. 1(e).

The defect modes are depicted by the red dashed lines in the band diagrams shown in Figs. 1(d) and 1(e). The optical defect mode was located inside the photonic bandgap of the P-I structure. However, the shrinkage of the radii of the air holes and the spacings between the holes contributed to a mechanical defect mode with a higher frequency, which exceeded the phononic bandgap of the P-I structure. Nevertheless, given that the frequency of the mechanical defect mode was located inside the mechanical bandgap of the P-II structure, the cavity confined the mechanical mode by the hetero OMC. Therefore, the optical and mechanical modes were confined separately by the P-I and P-II structures using the hetero OMC cavity.

B. Fabrication and Measurement of the Hetero OMC Cavity

To verify the degree and effectiveness of the mode confinement in the hetero structure, we fabricated three different cavity structures for comparison: i) a hetero OMC cavity; ii) an optomechanical cavity without a hetero structure; and iii) an optomechanical cavity with an acoustic radiation shield. The acoustic radiation shield [30] was a 2D cross periodic structure, which was capable of providing a complete phononic bandgap between 5.16 and 6.41 GHz.

All patterned structures were first defined by electron beam lithography (EBL) and transferred to the device layer of silicon-on-insulator (SOI) chips by inductively coupled plasma (ICP) etching. For the tapered-fiber-coupled cavities, the dry-etched structures were directly wet-etched by buffered hydrofluoric acid (BHF) to form suspended structures before the measurements.

Top-view scanning electron microscopy (SEM) images of the three different structures are given in Figs. 2(a)–2(c). They were probed by a tapered fiber in an ambient environment, and their optical and mechanical spectra are shown in Figs. 2(d) and 2(e). Herein, a tunable laser light source was used. For both measurement schemes, the output was split into two channels. One port was connected to a low-frequency optical power monitor, which acquired the optical spectrum by sweeping the wavelength of the laser. The other port was connected to a high-frequency (12.5 GHz) optical receiver, and its output was connected to an electrical spectrum analyzer to obtain the mechanical spectra.

The optical spectra show that all three cavity types possessed similar optical and mechanical frequencies, and similar optical Q-factors of the order of 10^4. We compared the intrinsic mechanical Q-factors for the three different cavities, which are important parameters for evaluating the confinement of the mechanical modes. Because the curves are all measured with a large detuning, the measured Q-factor can be approximate to the intrinsic mechanical Q value. Here, the mechanical Q-factor of the OMC cavity without a hetero structure was 2.6×10^2, which was much smaller than the values of the hetero OMC cavity and the OMC cavity with a radiation shield, both of which yielded a mechanical Q-factor of approximately 1.8×10^3. This indicates that the acoustic waves leaking through the P-I structure were blocked by the outer periodic structures of the hetero OMC cavity and by the OMC cavity with an acoustic radiation shield, while the P-II structure of the hetero OMC led to a confinement effect similar to that of the acoustic radiation shield in an ambient environment. As a result, the optical and mechanical modes were successfully confined separately by the two periodic structures in the hetero OMC cavity and by the OMC cavity with an acoustic radiation shield, which had been extensively used for OMCs [30,31].
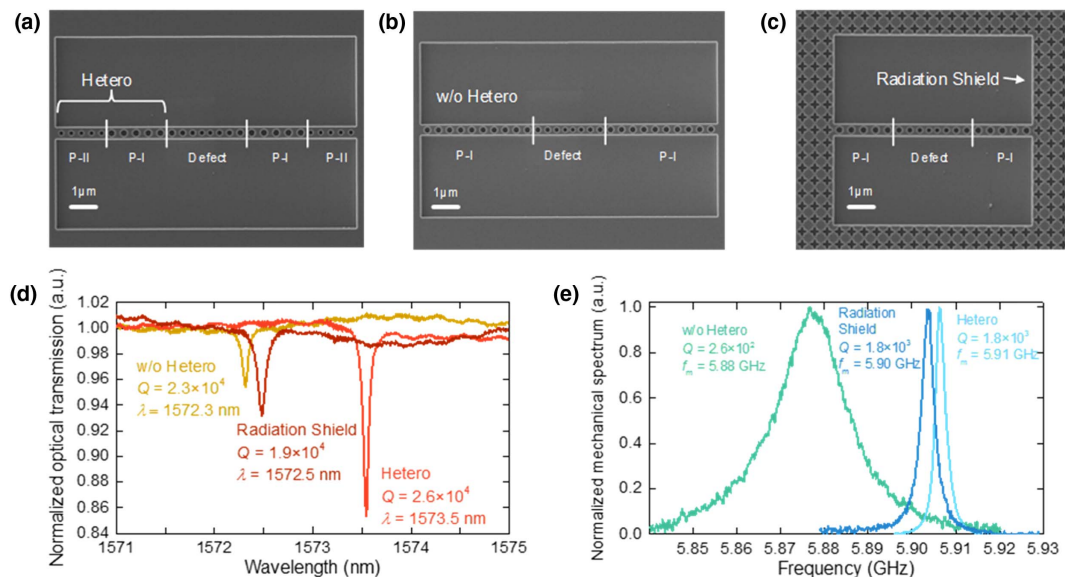

Fig. 2. Top-view scanning electron microscopy (SEM) images of the (a) hetero OMC cavity, (b) OMC cavity without a hetero structure, and (c) OMC cavity with radiation shield. (d) Optical and (e) mechanical spectra of the three types of OMC cavities.

Compared with the 2D acoustic radiation shield, the hetero OMC cavity designed with a 1D nanobeam structure is more suitable for use in integrated circuits.

In addition, thanks to the design flexibility offered by the separate confinement of the optical and mechanical modes in the hetero structure, we were able to demonstrate strong optomechanical coupling. The optomechanical coupling rate of the cavity was measured with the assistance of an electro-optic modulator for calibration. The measured optomechanical coupling rate ($g_0/2\pi$) of the cavity was 1.9 MHz.

C. Discussion of Phonon Laser Sensing in the Hetero OMC Cavity

Owing to the good confinement of the mechanical mode and the large optomechanical coupling rate, phonon lasing was demonstrated in the hetero OMC cavity [Fig. 3(a)] with low-coupled optical power. Figure 3(b) shows the normalized phonon number of the hetero OMC as a function of the coupled optical power when the pump light is blue-detuned. Herein, the phonon number is normalized to that excited by the thermal environment, which is equal to 1.06×10^3 at room temperature. The measured threshold of the coupled optical

power was 31 µW. Above this threshold, the mechanical linewidth is dramatically suppressed, reducing from 3.3 MHz to 5.2 kHz, as shown in Fig. 3(c), which corresponds to an effective mechanical Q-factor boosting from 1.8×10^3 to 1.1×10^6.

This suggests that the sensing resolution of the sensing mechanisms that rely on the detection of the frequency shift of the mechanical resonator can be greatly improved by the coherently narrowed mechanical linewidth that arises after phonon lasing. Given that the mechanical frequency of the phonon laser will shift with detuning between the pump light and the optical resonance owing to the optomechanical spring effect [3,17], the coherently enhanced sensing resolution can be analyzed as follows.

We now discuss the mechanism based on which our optomechanical cavity can be used to perform coherently enhanced sensing. When there is a small variation in the refractive index in the cavity's surroundings, such as a new particle that appears near the hetero cavity, the optical resonance of the cavity will shift and cause detuning between the fixed laser input and the optical resonance. Because the mechanical mode is sensitive to the detuning of the laser cavity that is induced by the optical
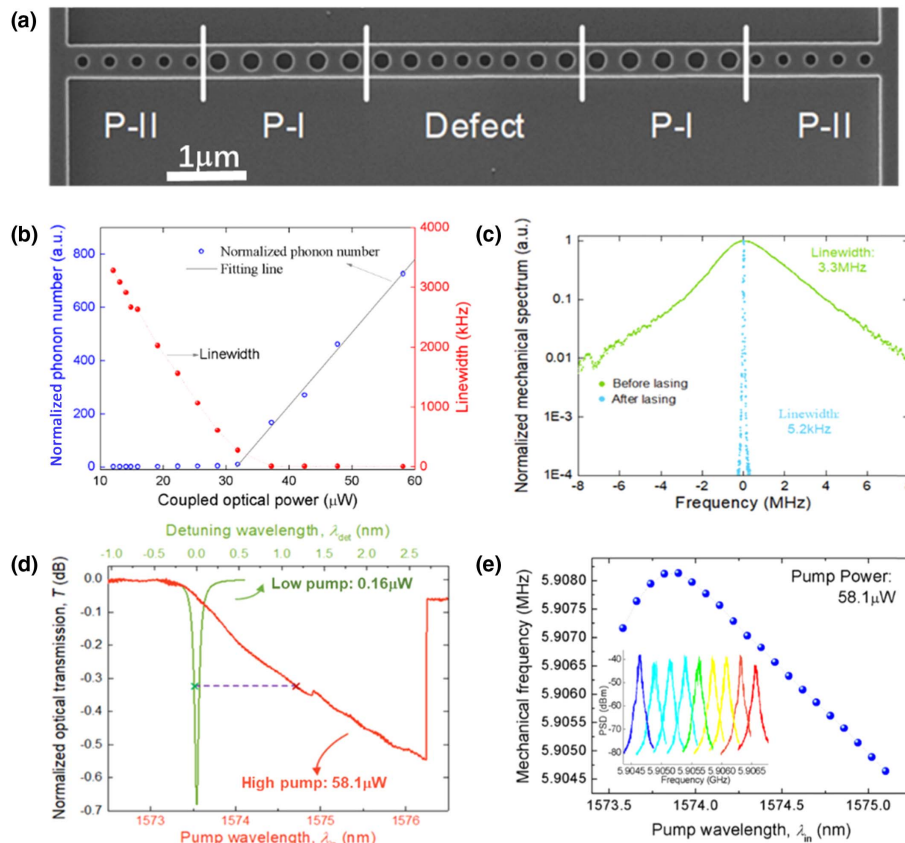

Fig. 3. (a) SEM image of the measured hetero OMC cavity. (b) Normalized phonon number and linewidth of the hetero OMC cavity as a function of coupled optical power. (c) Normalized mechanical spectra of the hetero OMC cavity before and after phonon lasing. (d) Normalized optical transmission for low- and high-pump power levels with pump power of 0.16 µW and 58.1 µW as a function of the pump wavelength and the detuning wavelength. The two crosses joined by the purple dashed line indicate the same detuning. Herein, the ratio between the optical detuning and optical decay rate was 0.50 when the linewidth of the mechanical spectrum achieved a minimum. (e) Measured mechanical frequency with pump power of 58.1 µW as a function of the pump wavelength. Inset shows the shift in mechanical peak under lasing at different pump wavelengths.
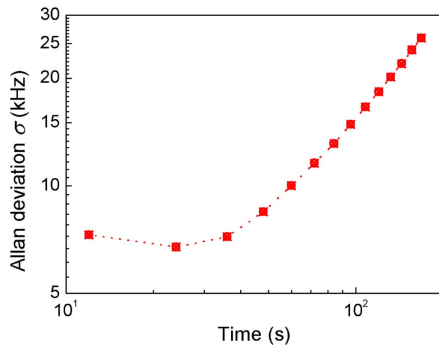
Fig. 4. Allan deviation of the fundamental mechanical mode after phonon lasing.

spring effect [3,17], the refractive index variation can be determined by measuring the mechanical frequency shift instead of the shift in the optical mode used in conventional methods [2,32]. However, in addition to the index variation, the optical frequency of the cavity will be redshifted owing to heat deposited when the OMC cavity is pumped with relatively high power to realize phonon lasing, as shown in Fig. 3(d). Thus, with a view to phonon laser sensing, two effects will lead to the resonance shift of the optical cavity and contribute to laser-cavity detuning. The first effect is the variation in the refractive index caused by a detected particle. The second is the change in the index due to the heat effect induced by increased pump power levels. The wavelength variation caused by the former effect needs to be determined for the purposes of practical sensing. The latter effect is that the phonon lasing above the threshold required a high pumping power causing non-negligible heating of the cavity. For this concern, we analyzed the heating effect using the method in Ref. [3], which reported experimental results for particle sensing with consideration of heating effect, and this can be deduced as follows:

$$\frac{d\lambda_{det}}{df_m} = \frac{d\lambda_{det}}{dT} \times \frac{dT}{d\lambda_{in}} \times \frac{d\lambda_{in}}{df_m}, \quad (1)$$

where λ_{det} is the detuning wavelength between the laser and the cavity resonance in the absence of heat effects, which corresponds to the resonance shift of the cavity caused by the small variation in the refractive index induced by a particle, T is the optical transmission power, λ_{in} is the pump-light wavelength, and f_m is the mechanical frequency.

Given that the same optical transmission at different pumping powers corresponds to the same level of detuning in the case of the optical cavity [3], the two crosses linked by the purple dashed line in Fig. 3(d) indicate equivalent detuning. Therefore, $dT/d\lambda_{det}$ and $dT/d\lambda_{in}$ can be deduced from the slope of the optical transmission in Fig. 3(d) based on our experiments. Their values were, respectively, equal to 20.9 and −0.195 dB/nm. A value of $d\lambda_{in}/df_m = 3.36 \times 10^{-4}$ nm/kHz was obtained from the measured mechanical frequency as a function of the pump wavelength in the linear region in Fig. 3(e). Herein, the mechanical peaks obtained with lasing at different pump wavelengths are also presented [inset of Fig. 3(e)]. Based on these parameters, the ratio $d\lambda_{det}/df_m$

was calculated to be equal to −3.1 × 10⁻⁶ nm/kHz via Eq. (1) for the demonstrated hetero cavity.

As the mechanical spectrum is dramatically narrowed after phonon lasing, the detectable mechanical frequency shift δf_m could be minimized to 5.2 kHz, thus yielding a wavelength resolution $\delta\lambda = (d\lambda_{det}/df_m) \times \delta f_m$ of 1.6×10^{-5} nm with $\lambda = 1572.3$ nm. Further, the Allan deviation [33] is used to characterize the frequency stability and analyze the sensing resolution. Here, we calculate the Allan deviation at time $m\tau_0$ $(m = 1, ..., N)$ as follows:

$$\sigma(m\tau_0) = \frac{1}{2(N - 2m + 1)} \sum_{j=1}^{N-2m+1} \left[\sum_{i=j}^{j+m-1} \left(\frac{f_{i+m} - f_i}{m} \right) \right]^2, \quad (2)$$

where τ_0 is the sample period; in our experiment, $\tau_0 = 12$ s. N is the total number of samples and $N = 32$. f_i is mechanical resonant frequency in the ith time interval of τ_0. The Allan deviation of the fundamental mechanical mode after the phonon lasing is measured with a minimum deviation of 6.7 kHz for our device (Fig. 4), which is the same level of lasing linewidth. Thus, the on-chip sensing with a resolution of $\delta\lambda/\lambda = 1.0 \times 10^{-8}$ is predicted in future sensing applications. This result represents an enhancement of three orders of magnitude compared with the mechanical linewidth of 3.3 MHz before phonon lasing. Furthermore, compared with other reported structures, such as silica microsphere [3,34,35] and microtoroid [36], the proposed silicon nanobeam OMC cavity with an ultrasmall motional mass (116 fg) and a small footprint can be easily integrated with other multifunctional on-chip devices, which is a good candidate for integrated sensing applications.

3. CONCLUSIONS

In this study, we have demonstrated that the use of hetero OMC cavities can separately confine the optical and mechanical modes using two types of periodic structures. Because the optical and mechanical modes were no longer confined by an identical periodic structure in conventional OMCs, the hetero structure led to the increased mechanical frequency of 5.91 GHz, which is much higher than that in our previous work [28,37,38] and contributes to increased resistance to environmental disturbances and to a larger sensing bandwidth while the optical mode was maintained at 1573.5 nm. The mechanical Q-factor of the hetero OMC was found to be 1.8×10^3, which was much higher than that of OMCs without a hetero structure (2.6×10^2) and close to that offered by OMCs with an acoustic radiation shield. This indicated that the optical and mechanical modes were well confined by the two periodic structures. The separate confinement mechanism introduced by the hetero structure was also responsible for boosting the coupling rate between the optical and mechanical modes, which was found to be as high as 1.9 MHz in the hetero cavity.

Pronounced phonon lasing has been shown to be viable for high-precision sensing applications based on a hetero OMC cavity, which was implemented in silicon. Owing to the coherence-related enhancement induced by the phonon lasing, the mechanical damping losses were dramatically reduced and led

to the narrowing of the linewidth in the range from 3.3 MHz to 5.2 kHz in an ambient environment. This corresponds to ultraprecise sensing with $\delta\lambda/\lambda = 1.0 \times 10^{-8}$. To this date, the largest optical Q-factor obtained for silicon-based photonic crystal microcavities is 10^7 [25] and corresponds to a sensing resolution of $\delta\lambda/\lambda \sim 10^{-7}$. We have thus demonstrated an improvement in the sensing resolution of one order of magnitude.

By coupling the hetero OMC cavity with an integrated evanescent coupling waveguide, the cavity could be readily used as a functional component and integrated with other on-chip devices for use in practical applications. Moreover, the mode confinement approach adopted here could be applied to 2D cavities [39] or waveguides [40] to further improve their mechanical properties.

Disclosures. The authors declare no conflicts of interest.

Data Availability. The data that support the plots within this paper and other findings are available from the corresponding author upon reasonable request.

†These authors contributed equally to this work.

REFERENCES

1. S. Olcum, N. Cermak, S. C. Wasserman, and S. R. Manalis, "High-speed multiple-mode mass-sensing resolves dynamic nanoscale mass distributions," Nat. Commun. **6**, 7070 (2015).
2. F. Liu, S. Alaie, Z. C. Leseman, and M. Hossein-Zadeh, "Sub-pg mass sensing and measurement with an optomechanical oscillator," Opt. Express **21**, 19555–19567 (2013).
3. W. Yu, W. C. Jiang, Q. Lin, and T. Lu, "Cavity optomechanical spring sensing of single molecules," Nat. Commun. **7**, 12311 (2016).
4. K. Jensen, K. Kim, and A. Zettl, "An atomic-resolution nanomechanical mass sensor," Nat. Nanotechnol. **3**, 533 (2008).
5. E. Gavartin, P. Verlot, and T. J. Kippenberg, "A hybrid on-chip optomechanical transducer for ultrasensitive force measurements," Nat. Nanotechnol. **7**, 509–514 (2012).
6. M. Wu, A. C. Hryciw, C. Healey, D. P. Lake, H. Jayakumar, M. R. Freeman, J. P. Davis, and P. E. Barclay, "Dissipative and dispersive optomechanics in a nanocavity torque sensor," Phys. Rev. X **4**, 021052 (2014).
7. J. D. Teufel, T. Donner, M. A. Castellanos-Beltran, J. W. Harlow, and K. W. Lehnert, "Nanomechanical motion measured with an imprecision below that at the standard quantum limit," Nat. Nanotechnol. **4**, 820–823 (2009).
8. M. Wu, N. L. Wu, T. Firdous, F. F. Sani, J. E. Losby, M. R. Freeman, and P. E. Barclay, "Nanocavity optomechanical torque magnetometry and radiofrequency susceptometry," Nat. Nanotechnol. **12**, 127–131 (2017).
9. B. Li, J. Bilek, U. B. Hoff, L. S. Madsen, S. Forstner, V. Prakash, C. Schafermeier, T. Gehring, W. P. Bowen, and U. L. Andersen, "Quantum enhanced optomechanical magnetometry," Optica **5**, 850–856 (2018).
10. S. Prams, J. Knittel, E. D. van Ooijen, J. D. Swaim, G. I. Harris, A. Szorkovszky, W. P. Bowen, H. Rubinsztein-Dunlop, and S. Forstner, "Cavity optomechanical magnetometer," Phys. Rev. Lett. **108**, 120801 (2012).
11. A. G. Krause, M. Winger, T. D. Blasius, Q. Lin, and O. Painter, "A high-resolution microchip optomechanical accelerometer," Nat. Photonics **6**, 768–772 (2012).
12. H. Rokhsari, T. Carmon, A. Scherer, K. J. Vahala, and T. J. Kippenberg, "Analysis of radiation-pressure induced mechanical oscillation of an optical microcavity," Phys. Rev. Lett. **95**, 033901 (2005).
13. E. Verhagen, S. Deléglise, S. Weis, A. Schliesser, and T. J. Kippenberg, "Quantum-coherent coupling of a mechanical oscillator to an optical cavity mode," Nature **482**, 63–67 (2012).
14. Z. Shen, Y. Zhang, Y. Chen, C. Zou, Y. Xiao, X. Zou, F. Sun, G. Guo, and C. Dong, "Experimental realization of optomechanically induced non-reciprocity," Nat. Photonics **10**, 657–661 (2016).
15. J. D. Thompson, B. M. Zwickl, A. M. Jayich, F. Marquardt, S. M. Girvin, and J. G. E. Harris, "Strong dispersive coupling of a high-finesse cavity to a micromechanical membrane," Nature **452**, 72–75 (2008).
16. M. Eichenfield, J. Chan, R. M. Camacho, K. J. Vahala, and O. Painter, "Optomechanical crystals," Nature **462**, 78–82 (2009).
17. T. J. Kippenberg, F. Marquardt, and M. Aspelmeyer, "Cavity optomechanics," Rev. Mod. Phys. **86**, 1391–1452 (2014).
18. J. Chan, T. Alegre, A. H. Safavi-Naeini, J. T. Hill, A. Krause, S. Groblacher, M. Aspelmeyer, and O. Painter, "Laser cooling of a nanomechanical oscillator into its quantum ground state," Nature **478**, 89–92 (2011).
19. E. Gil-Santos, C. Baker, D. T. Nguyen, W. Hease, C. Gomez, A. Lemaitre, S. Ducci, G. Leo, and I. Favero, "High-frequency nano-optomechanical disk resonators in liquids," Nat. Nanotechnol. **10**, 810–816 (2015).
20. K. L. Ekinci, Y. T. Yang, and M. L. Roukes, "Ultimate limits to inertial mass sensing based upon nanoelectromechanical systems," J. Appl. Phys. **95**, 2682–2689 (2004).
21. A. N. Cleland and M. L. Roukes, "Noise processes in nanomechanical resonators," J. Appl. Phys. **92**, 2758–2769 (2002).
22. G. Anetsberger, E. Gavartin, O. Arcizet, Q. P. Unterreithmeier, E. M. Weig, M. L. Gorodetsky, J. P. Kotthaus, and T. J. Kippenberg, "Measuring nanomechanical motion with an imprecision below the standard quantum limit," Phys. Rev. A **82**, 820–823 (2010).
23. G. Anetsberger, O. Arcizet, Q. P. Unterreithmeier, R. Riviere, A. Schliesser, E. M. Weig, J. P. Kotthaus, and T. J. Kippenberg, "Near-field cavity optomechanics with nanomechanical oscillators," Nat. Phys. **5**, 909–914 (2009).
24. K. Srinivasan, H. Miao, M. T. Rakher, M. Davanco, and V. Aksyuk, "Optomechanical transduction of an integrated silicon cantilever probe using a microdisk resonator," Nano Lett. **11**, 791–797 (2011).
25. T. Asano, Y. Ochi, Y. Takahashi, K. Kishimoto, and S. Noda, "Photonic crystal nanocavity with a Q factor exceeding eleven million," Opt. Express **25**, 1769–1777 (2017).
26. J. L. Arlett, E. B. Myers, and M. L. Roukes, "Comparative advantages of mechanical biosensors," Nat. Nanotechnol. **6**, 203–215 (2011).

27. K. Vahala, M. Herrmann, S. Knünz, V. Batteiger, G. Saathoff, T. W. Hänsch, and T. Udem, "A phonon laser," Nat. Phys. **5**, 682–686 (2009).
28. F. Pan, K. Cui, G. Bai, X. Feng, F. Liu, W. Zhang, and Y. Huang, "Radiation-pressure-antidamping enhanced optomechanical spring sensing," ACS Photon. **5**, 4164–4169 (2018).
29. Z. Huang, K. Cui, Y. Li, X. Feng, F. Liu, W. Zhang, and Y. Huang, "Strong optomechanical coupling in nanobeam cavities based on hetero optomechanical crystals," Sci. Rep. **5**, 15964 (2015).
30. J. Chan, A. H. Safavi-Naeini, J. T. Hill, S. Meenehan, and O. Painter, "Optimized optomechanical crystal cavity with acoustic radiation shield," Appl. Phys. Lett. **101**, 081115 (2012).
31. K. C. Balram, M. I. Davanco, J. D. Song, and K. Srinivasan, "Coherent coupling between radiofrequency, optical and acoustic waves in piezo-optomechanical circuits," Nat. Photonics **10**, 346–352 (2016).
32. K. Han, J. Kim, and G. Bahl, "High-throughput sensing of freely flowing particles with optomechanofluidics," Optica **3**, 585–591 (2016).
33. S. Olcum, N. Cermak, S. C. Wasserman, K. Christine, S. H. Atsumi, K. R. Payer, W. Shen, J. Lee, A. M. Belcher, S. N. Bhatia, and S. R. Manalisa, "Weighing nanoparticles in solution at the attogram scale," Proc. Natl. Acad. Sci. USA **111**, 1310–1315 (2014).
34. Z. Shen, Z. Zhou, C. Zou, F. Sun, G. Guo, C. Dong, and G. Guo, "Observation of high-Q optomechanical modes in the mounted silica microspheres," Photon. Res. **3**, 243–247 (2015).
35. G. Qin, M. Wang, J. Wen, R. Dong, and G. Long, "Brillouin cavity optomechanics sensing with enhanced dynamical backaction," Photon. Res. **7**, 1440–1446 (2019).
36. B. Li, G. Brawley, H. Greenall, S. Forstner, and W. P. Bowen, "Ultrabroadband and sensitive cavity optomechanical magnetometry," Photon. Res. **8**, 1064–1071 (2020).
37. Y. Li, K. Cui, X. Feng, Z. Huang, F. Liu, W. Zhang, and Y. Huang, "Optomechanical crystal nanobeam cavity with high optomechanical coupling rate," J. Opt. **17**, 045001 (2015).
38. Z. Huang, K. Cui, G. Bai, X. Feng, F. Liu, W. Zhang, and Y. Huang, "High-mechanical-frequency characteristics of optomechanical crystal cavity with coupling waveguide," Sci. Rep. **6**, 34160 (2016).
39. A. H. Safavi-Naeini, J. T. Hill, S. Meenehan, J. Chan, S. Groeblacher, and O. Painter, "Two-dimensional phononic-photonic band gap optomechanical crystal cavity," Phys. Rev. Lett. **112**, 153603 (2014).
40. A. H. Safavi-Naeini and O. Painter, "Design of optomechanical cavities and waveguides on a simultaneous bandgap phononic-photonic crystal slab," Opt. Express **18**, 14926–14943 (2010).